nature chemistry

Article

https://doi.org/10.1038/s41557-024-01511-2

# Proton-triggered topological transformation in superbase-mediated selective polymerization enables access to ultrahigh-molar-mass cyclic polymers

Received: 19 June 2023

Accepted: 18 March 2024

Published online: 22 April 2024

Check for updates

Li Zhou, Liam T. Reilly, Changxia Shi, Ethan C. Quinn & Eugene Y.-X. Chen

The selective synthesis of ultrahigh-molar-mass (UHMM, >2 million Da) cyclic polymers is challenging as an exceptional degree of spatiotemporal control is required to overcome the possible undesired reactions that can compete with the desired intramolecular cyclization. Here we present a counterintuitive synthetic methodology for cyclic polymers, represented here by polythioesters, which proceeds via superbase-mediated ring-opening polymerization of *gem*-dimethylated thiopropiolactone, followed by macromolecular cyclization triggered by protic quenching. This proton-triggered linear-to-cyclic topological transformation enables selective, linear polymer-like access to desired cyclic polythioesters, including those with UHMM surpassing 2 MDa. In addition, this method eliminates the need for stringent conditions such as high dilution to prevent or suppress linear polymer contaminants and presents the opposite scenario in which protic-free conditions are required to prevent cyclic polymer formation, which is capitalized to produce cyclic polymers on demand. Furthermore, such UHMM cyclic polythioester exhibits not only much enhanced thermostability and mechanical toughness, but it can also be quantitatively recycled back to monomer under mild conditions due to its *gem*-disubstitution.

Cyclic polymers have continued to attract much attention in polymer science due to their unique loop topology and still unmet synthetic challenges in preparing them in high molar mass and purity, and in a controlled fashion[1–6]. Without chain ends, cyclic polymers exhibit unique physical, rheological and thermal properties relative to their linear counterparts[7–12]. Notable progress has been made to understand cyclic polymers' topologically enabled properties, revealing their unique applications in biomedicine[13–16], microelectronics[17,18] and material science[19,20]. The cyclic structure is traditionally accessed through ring closing or ring expansion mechanisms. The former approach typically requires high dilution or is otherwise plagued by the lack of control over molar mass and dispersity[21–23]. The latter method requires specific catalysts or initiating species, and such suitable catalysts have been reported and successfully used in ring-opening olefin metathesis[24–29] and Lewis pair polymerization[30–32].

Numerous examples using ring-opening polymerization (ROP) of heterocyclic monomers to produce cyclic polymers via in situ cyclization of propagating species have been reported[33–40]. However, regardless of whether the ROP is organically initiated zwitterionic[33–35] or metal-catalysed coordinative-insertion mechanisms[39,40], the enabling

Department of Chemistry, Colorado State University, Fort Collins, CO, USA. e-mail: eugene.chen@colostate.edu

https://doi.org/10.1038/s41557-024-01511-2

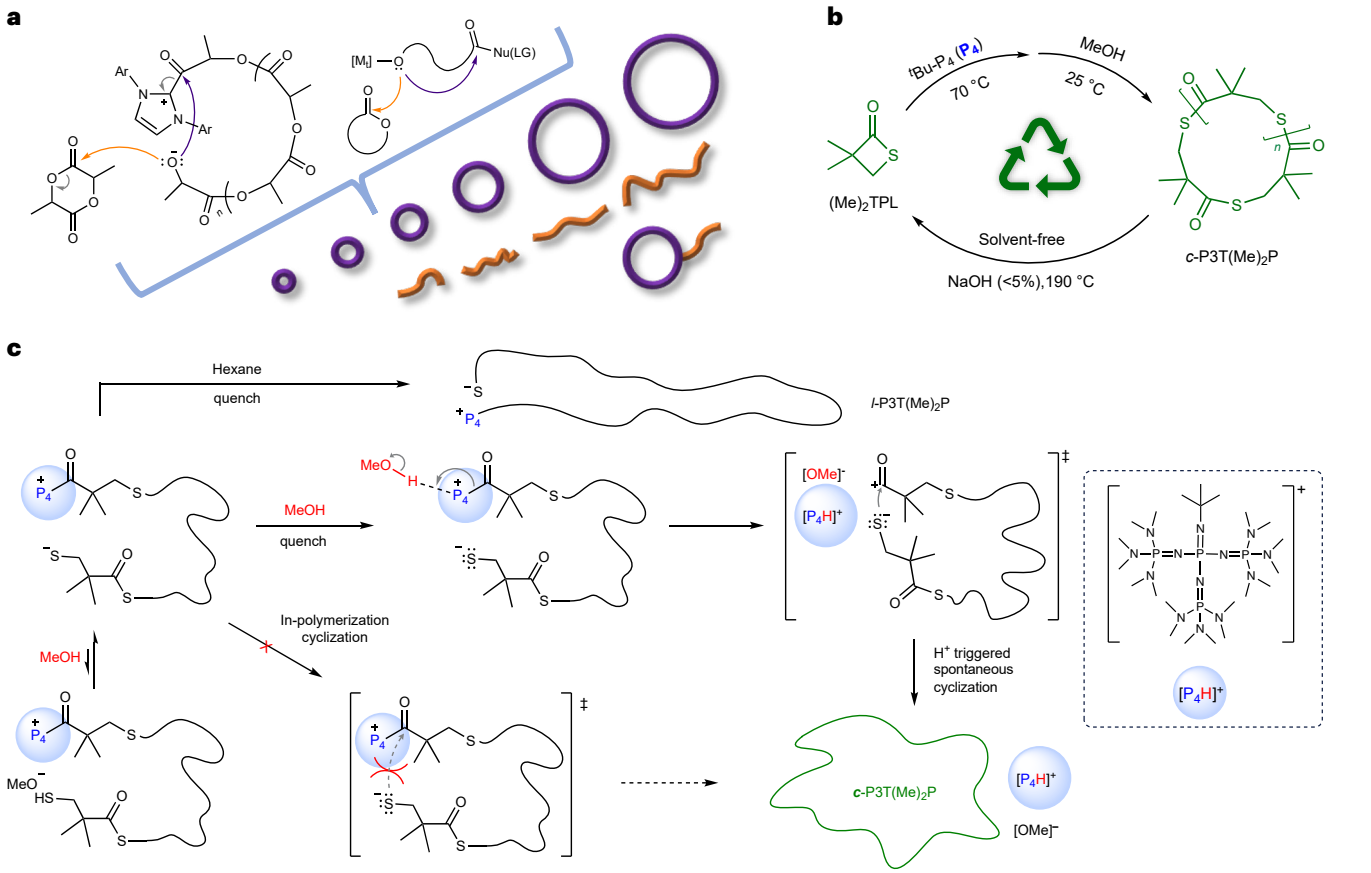


**Fig. 1 | Proton-triggered cyclization versus in-polymerization cyclization.** **a**, Outlined common challenges in the synthesis of cyclic polymers due to competing linear-chain propagation (orange arrow) and cyclization (purple arrow) processes leading to structural heterogeneity (purple rings and orange open chains). **b**, Chemically circular cyclic P3T(Me)$_2$P through $^t$Bu–P$_4$-mediated ROP and protic quenching, as well as catalysed recycling to monomer with NaOH. **c**, Proposed mechanism for macromolecular cyclization triggered by a protic reagent MeOH (shown in red). In-polymerization cyclization is sterically blocked by the bonded bulky superbase ($^t$Bu–P$_4$) moiety. However, the detachment of this bulky superbase on protonation allows cyclization to occur, producing *c*-P3T(Me)$_2$P with excellent properties ($M_n$ = 2.23 MDa, $\sigma_b$ = 39.3 MPa, $\varepsilon_b$ = 282%). The structure of the leaving group [P$_4$H]$^+$ is enclosed in a box with a dashed border.

step is in-polymerization cyclization (polymerization and cyclization events occur concurrently) of a growing chain, which always competes with linear-chain propagation, thus often resulting in formation of cyclic polymers with uncontrolled molar mass and high dispersity (that is, forming rings in large size variations) as well as linear contaminants (Fig. 1a). Using such existing methods to access cyclic polymers with ultrahigh-molar-mass (UHMM, defined here as number-average molar mass ($M_n$) >2 million daltons (MDa)) and in high selectivity is particularly challenging, due to competing propagation and/or cyclization processes and other side reactions such as chain transfer or termination under high monomer-to-initiator and/or catalyst conditions. Ideally, if cyclization occurs only when an external trigger is applied, then cyclic polymers should be synthesizable in the same manner as linear counterparts, thereby accessing cyclic polymers with the same precision and designability as the linear ones, including UHMM cyclic polymers with low dispersity ($Đ$ < 1.4).

To realize this intriguing possibility and demonstrate the concept, we arrived to the organic ROP of 2,2-dimethyl-3-thiopropiolactone ((Me)$_2$TPL) aiming for the corresponding cyclic polythioester, poly (2,2-dimethyl-3-thiopropiolactone) (*c*-P3T(Me)$_2$P) (Fig. 1b), on the basis of the following four hypotheses. First, cyclic, sulfur-containing polythioester with UHMM may provide a unique opportunity for direct visualization by microscopies such as atomic force microscopy (AFM), thus eliminating the need for postpolymerization functionalization via thiol-ene click to enable visualization[30,31,41]. Second, owing to the lability of thioester bonds, back-biting cyclization via transthioesterification should be more facile than transesterification of polyester chains, facilitating cyclic polythioester formation. This reasoning was beautifully demonstrated by the recent work of Guillaume and Carpentier showing that the metal-mediated ROP of an analogous four-membered thiolactone, (±)-β-thiobutyrolactone, forms cyclic poly(3-thiobutyrolactone) (*c*-P3TB) enabled by in-polymerization back-biting cyclization[42]. Isotactic and syndiotactic *c*-P3TB materials were synthesized using different yttrium-based catalysts, but the reported $M_n$ was only up to 46.5 kDa and the recycling of P3TB to monomer was not demonstrated. Obtaining cyclic polymers with high molar mass and the ability to be recycled back to a monomer (known as chemical circularity) is essential for achieving high-performance materials and circular economy[43–47]. Third, installation of α,α-*gem*-dimethyl groups to the thiopropiolactone ring should increase the depolymerizability of the polythioester back to its thiolactone monomer by shifting the polymer–monomer equilibrium towards the monomer through the Thorpe–Ingold effect[48], thus establishing chemical circularity of *c*-P3T(Me)$_2$P (Fig. 1b). This *gem*-disubstitution effect has been successfully applied to several strained (thio)lactones to enable their corresponding poly(thio)esters to be chemically circular[49–52]. Fourth, suppression or elimination of in-polymerization cyclization could be achieved by using an exceptionally bulky (~1.4 nm) phosphazene superbase, $^t$Bu–P$_4$ (((Me$_2$N)$_3$P=N))$_3$P=N($^t$Bu))[53], which is posited to effectively block the cyclization during the polymerization (Fig. 1c). However, when it is detached from

https://doi.org/10.1038/s41557-024-01511-2

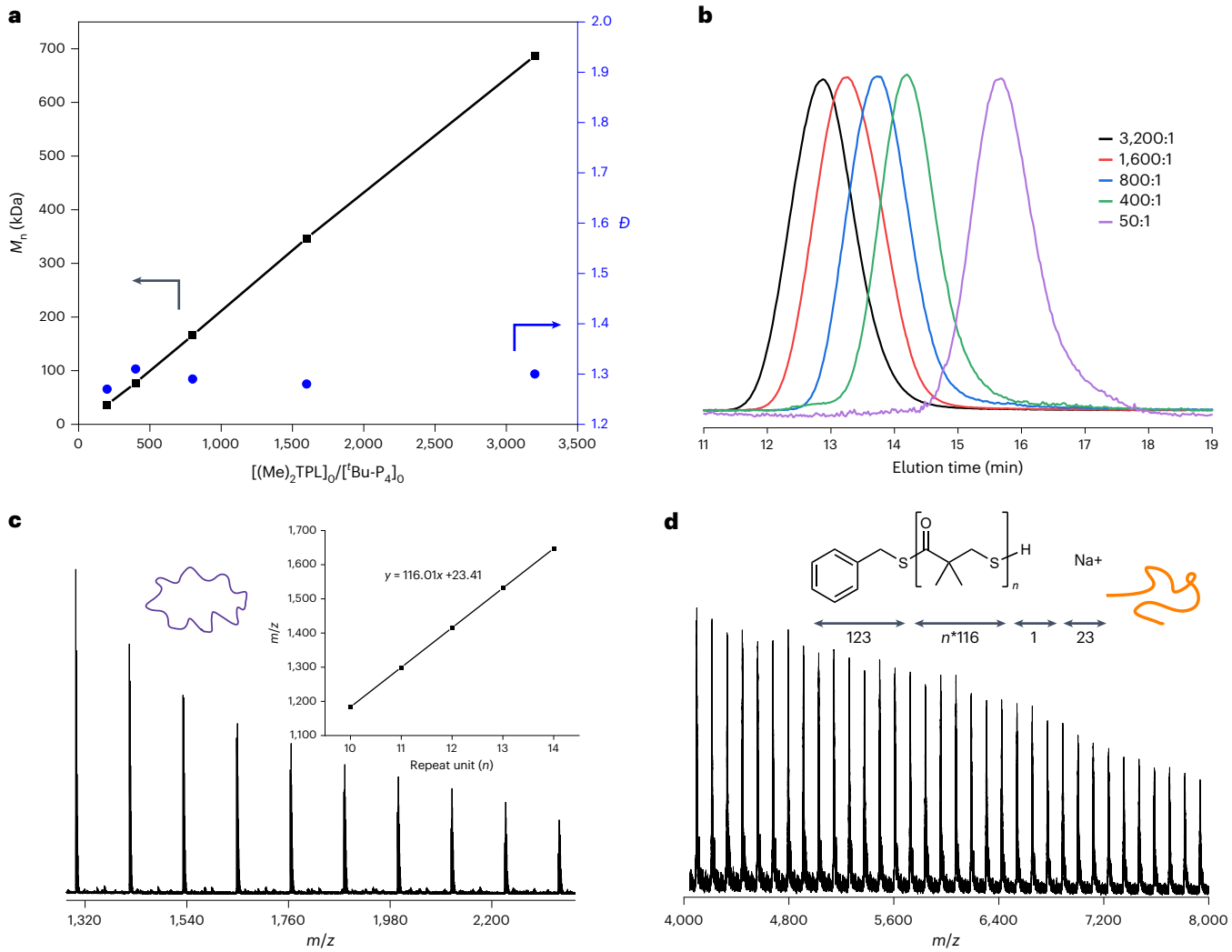


**Fig. 2 | Evidence for the controlled synthesis *l*- and *c*-P3T(Me)$_2$P. a**, Plot of $M_n$ and $Đ$ values of *c*-P3T(Me)$_2$P as a function of the ((Me)$_2$TPL):($^t$Bu−P$_4$) ratio; $M_n$ is shown in black and $Đ$ in blue. **b**, SEC curves for the *c*-P3T(Me)$_2$P samples produced at the different ((Me)$_2$TPL):($^t$Bu−P$_4$) ratio. **c**, MALDI–TOF–MS spectrum of *c*-P3T(Me)$_2$P produced with ((Me)$_2$TPL):($^t$Bu−P$_4$) = 50:1; the inset is the plot of *m/z* values versus the number of (Me)$_2$TPL repeat units. The series of molecular ion peaks are assigned to the *c*-P3T(Me)$_2$P without no chain ends ($M_{end}$ = 0 + 23 ($Na^+$) g mol$^{-1}$). **d**, MALDI–TOF–MS spectrum of *l*-P3T(Me)$_2$P produced with ((Me)$_2$TPL):(DBU):(BnSH) = 50:1:1; * denotes 'times'.

the chain, simply triggered by a protic quenching reagent, such as $H^+$/MeOH or MeOH at the end of polymerization, due to its high Brønsted basicity but relatively low nucleophilicity[54], spontaneous cyclization takes place to furnish the desired *c*-P3T(Me)$_2$P (Fig. 1c). Guided by the above four hypotheses, we achieved results, described as follows, demonstrating that the $^t$Bu−P$_4$-mediated ROP of (Me)$_2$TPL does indeed selectively produce *c*-P3T(Me)$_2$P with UHMM ($M_n$ = 2.23 MDa) through the proposed macromolecular cyclization by a protic trigger, and it is fully recyclable to a monomer.

## Result and discussion

### Organocatalyst-controlled topology P3T(Me)$_2$P

The monomer (Me)$_2$TPL can be synthesized in good yield via a two-step process from commercially available 3-chloropivalic acid (Supplementary Methods) or, more importantly, is obtainable in high yield (up to 95%) from NaOH-catalysed bulk depolymerization of UHMM P3T(Me)$_2$P at 190 °C (vide infra). Initial polymerization screenings used organic bases including superbases $^t$Bu−P$_4$, Et$_3$N and 1,8-diazabicyclo [5.4.0]undec-7-ene (DBU) in tetrahydrofuran (THF) at 70 °C (Supplementary Table 1). Polymerization runs with $^t$Bu−P$_4$ were conducted across a range of ((Me)$_2$TPL):($^t$Bu−P$_4$) ratios from 200:1 to 3,200:1. The size-exclusion chromatography (SEC) analysis of the resulting polymers revealed a linear and proportional increase of molar mass ($M_n$ = 36.7–687 kDa) with the increase of the ((Me)$_2$TPL):($^t$Bu−P$_4$) ratio, while the dispersity remained relatively narrow ($Đ$ = 1.27–1.31), evidencing a controlled polymerization (Fig. 2a,b). The ROP of (Me)$_2$TPL by $^t$Bu−P$_4$ at a ratio of 6,400:1 afforded UHMM P3T(Me)$_2$P ($M_n$ = 2.23 MDa, $Đ$ = 1.34). Matrix-assisted laser desorption–ionization time-of-flight–mass spectroscopy (MALDI–TOF–MS) analysis of the low-molar-mass P3T(Me)$_2$P using ((Me)$_2$TPL):($^t$Bu−P$_4$) = 50:1 showed a single series of molecular ion peaks corresponding to a repeating unit mass of 116 Da and no end groups, indicating the prospective formation of *c*-P3T(Me)$_2$P (Fig. 2c and Supplementary Fig. 1).

To further characterize the topology of the proposed *c*-P3T(Me)$_2$P, we attempted to synthesize a linear analogue[55], *l*-P3T(Me)$_2$P, for comparative analysis. We proposed that substituting the initiating $^t$Bu−P$_4$ with a species of a lower propensity for displacement in the ring closing attack of the α terminus by the anionic ω terminus would suppress the formation of *c*-P3T(Me)$_2$P and result in the formation of *l*-P3T(Me)$_2$P. Additionally, an initiating species that does not electrostatically draw the termini into proximity and proceeds through an ion-paired or neutral, rather than zwitterionic, polymerization should further inhibit the

https://doi.org/10.1038/s41557-024-01511-2

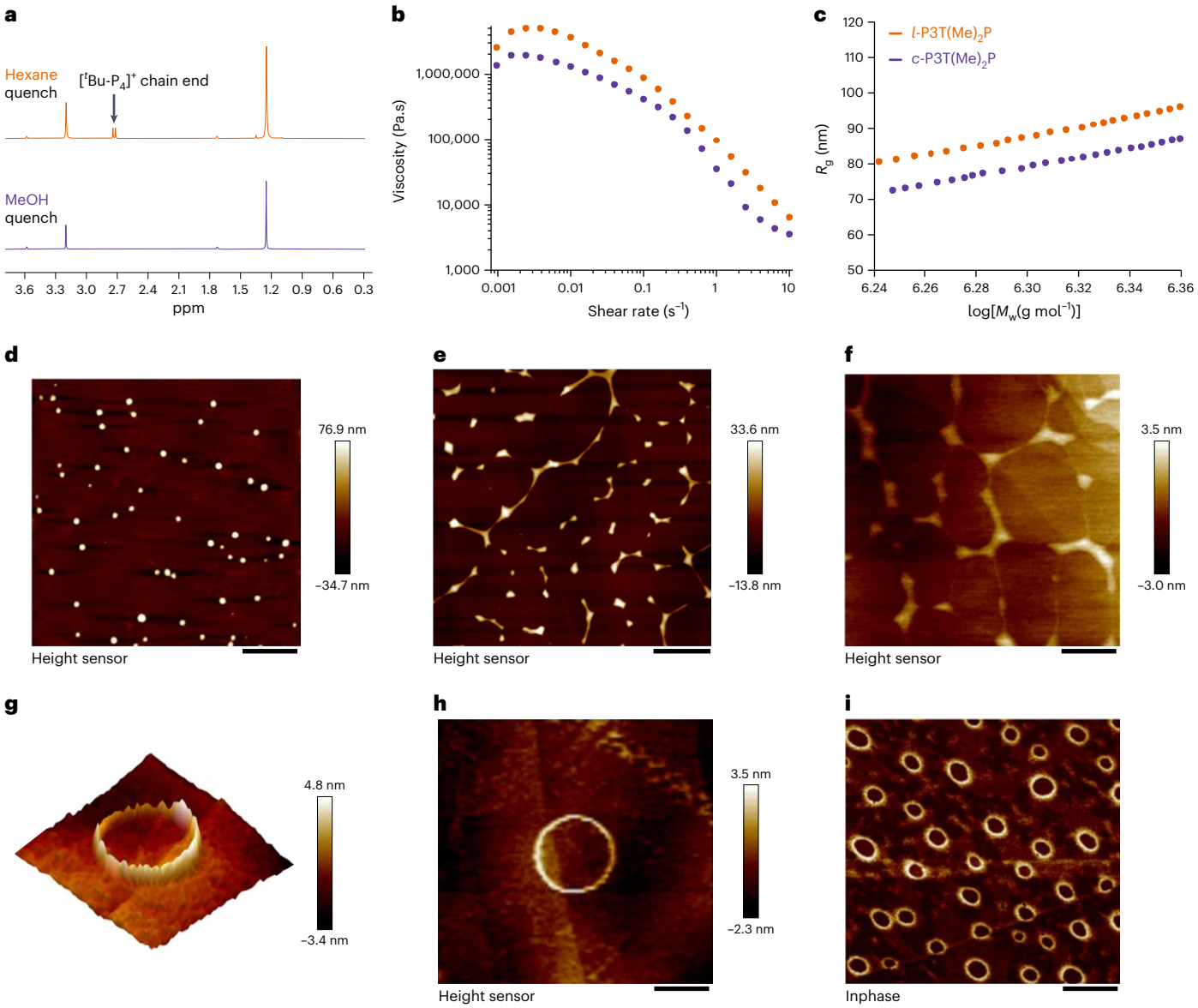


**Fig. 3 | Comparative characterizations of linear (orange lines) and cyclic (purple lines) P3T(Me)$_2$P prepared by different quenching methods.** **a**, Different quenching methods yield different topologies through end-group analysis by $^1$H NMR (THF-$d_8$). **b**, Rheological shear viscosities of UHMM *l*- and *c*-P3T(Me)$_2$P. **c**, Plots of $R_g$ versus log($M_w$) showing lower $R_g$ for the cyclic polymer, *c*-P3T(Me)$_2$P ($M_n$ = 2.22 MDa) than the linear counterpart, *l*-P3T(Me)$_2$P ($M_n$ = 2.17 MDa). **d**, Two-dimensional height sensor data collected from AFM analysis of *c*-P3T(Me)$_2$P (1.0 mg ml$^{-1}$, 2,000 rpm); polymer aggregates are discerned by the observed heights, approximately 77 nm for *c*-P3T(Me)$_2$P. Scale bar, 5.0 µm. **e**, Two-dimensional height sensor data collected from AFM analysis of comparative *l*-P3T(Me)$_2$P (1.0 mg ml$^{-1}$, 2,000 rpm); polymer aggregates are discerned by the observed heights, approximately 34 nm for *l*-P3T(Me)$_2$P. Scale bar, 2.0 µm. **f**, Two-dimensional height sensor data collected from AFM analysis of comparative *l*-P3T(Me)$_2$P (0.01 mg ml$^{-1}$, 4,000 rpm). Scale bar, 700 nm. **g**, Three-dimensional height sensor data collected from AFM analysis of *c*-P3T(Me)$_2$P (0.01 mg ml$^{-1}$, 4,000 rpm). **h**, Two-dimensional height sensor data collected from AFM analysis of comparative *c*-P3T(Me)$_2$P (0.01 mg ml$^{-1}$, 4,000 rpm). Scale bar, 700 nm. **i**, Two-dimensional in-phase phase shift data collected from AFM analysis of *c*-P3T(Me)$_2$P (0.01 mg ml$^{-1}$, 4,000 rpm). Scale bar, 850 nm.

formation of cyclic products. To this end, benzyl alcohol (BnOH) was used as the co-initiator. Before monomer addition, BnOH was premixed with $^t$Bu–P$_4$ in a 1:1 ratio and stirred for 10 minutes to ensure formation of the corresponding benzyl alkoxide. MALDI–TOF–MS analysis of the P3T(Me)$_2$P obtained from the ((Me)$_2$TPL):($^t$Bu–P$_4$):(BnOH) = 50:1:1 ratio run produced a mass spectrum with the major peaks matching those of the P3T(Me)$_2$P produced by $^t$Bu–P$_4$ alone (Supplementary Fig. 2). Switching to the mercaptan equivalent (BnSH) resulted in a mixture of different end groups (Supplementary Fig. 3). We therefore opted for a weaker nucleophilic base (Et$_3$N) that would not compete with BnSH for initiation of the ROP of (Me)$_2$TPL with ((Me)$_2$TPL):(Et$_3$N):(BnSH) = 50:1:1 and satisfyingly observed the formation of *l*-P3T(Me)$_2$P ($M_n$ = 7.2 kDa, $Đ$ = 1.37) with a single end-group set corresponding to the mass of BnSH (Supplementary Fig. 4). However, the rate of polymerization (86% conversion after 96 h ((Me)$_2$TPL):(Et$_3$N):(BnSH) = 200:1:1) proved too slow for the efficient synthesis of high molar mass samples. This is most probably a result of an equilibrium proton exchange between the active anionic chain end and Et$_3$N-H$^+$, thus impeding the rate of propagation. In light of this reasoning, the stronger base DBU was used. Quantitative monomer conversion was achieved within 12 h with ((Me)$_2$TPL):(DBU):(BnSH) = 200:1:1, corresponding to a greater than eight times increase in rate relative to the Et$_3$N runs. MALDI–TOF–MS analysis of the P3T(Me)$_2$P ($M_n$ = 6.4 kDa, $Đ$ = 1.33) obtained from a run with ((Me)$_2$TPL):(DBU):(BnSH) = 50:1:1 confirmed the linear topology with a single end-group

set corresponding to the mass of BnSH (Fig. 2d and Supplementary Fig. 5). The control of the DBU–BnSH polymerization was confirmed by SEC analysis across a range of initiator loadings from ((Me)$_2$TPL):(DBU):(BnSH) = 50:1:1 to 200:1:1, which revealed a linear and proportional relationship between molar mass and the ((Me)$_2$TPL):(BnSH) ratio, while the dispersity of the resulting linear P3T(Me)$_2$P remained relatively narrow (1.33–1.49) (Supplementary Fig. 6). Lowering the DBU catalyst loading to 0.06 mol% (((Me)$_2$TPL):(DBU):(BnSH) = 1,600:1:1), a high-molar-mass *l*-P3T(Me)$_2$P (129 kDa, $Đ$ = 1.35) was afforded. Having achieved the synthetic route to *l*-P3T(Me)$_2$P, analogous *c*- and *l*-P3T(Me)$_2$P were subsequently synthesized by their respective initiating system ($^t$Bu–P$_4$ and DBU–BnSH) with similar molar mass and dispersity values (*c*-P3T(Me)$_2$P: $M_n$ = 16.0 kDa, $Đ$ = 1.35; *l*-P3T(Me)$_2$P: $M_n$ = 17.1 kDa, $Đ$ = 1.60, Supplementary Fig. 7). A Mark–Houwink–Sakurada plot (that is, double logarithmic plots of intrinsic viscosity ([$\eta$]) versus weight-average molar mass ($M_w$) determined by light scattering detection) confirmed the *c*-P3T(Me)$_2$P exhibited a lower [$\eta$] than its linear counterpart (Supplementary Fig. 8), further supporting the topological assignments.

## Controlling the topology by different quenching methods

The above observed excellent selectivity, control over molar mass and narrow dispersity for the synthesized *c*-P3T(Me)$_2$P led to a hypothesis that the chain cyclization event occurs after complete conversion of the monomer. Two plausible explanations could account for this scenario: the first being that the mechanism of cyclization is available throughout the polymerization reaction, but the rate of this event is too slow to compete with propagation. Alternatively, the cyclization pathway is inaccessible before full monomer conversion and addition of an external trigger such as the protic quench or workup that catalyses the topological transformation. We produced the following four lines of evidence that are consistent with the latter scenario. First, the rate of polymerization was not observed to be particularly fast and several runs that were analysed before complete monomer conversion also possessed narrow dispersity and cyclic topology after the protic quench. Second, $^1$H nuclear magnetic resonance (NMR) (THF-$d_8$) analysis of the polymer sample obtained from quenching the polymerization with ((Me)$_2$TPL):($^t$Bu–P$_4$) = 50:1 in a non-protic solvent such as hexane clearly revealed the $^t$Bu–P$_4$ chain end (Fig. 3a and Supplementary Figs. 13 and 15). This chain-end evidence revealed by $^1$H NMR was further corroborated by $^{13}$P NMR spectra that showed the $^t$Bu–P$_4$ chain end is well located on the polymer chain quenched in hexane (Supplementary Fig. 16), supporting a linear topology without cyclization. Third, in contrast, no chain end was observed in the polymer sample quenched with protic MeOH or acidified MeOH (Fig. 3a and Supplementary Fig. 14). Note that, to exclude the potential interference of the possibly consumed initiator $^t$Bu–P$_4$, all isolated polymers before NMR analyses were precipitated twice in hexane or methanol and dried.

This unique, selective and convenient quenching method for topological transformation enabled us to synthesize both UHMM linear and cyclic polymers in parallel. Specifically, we carried out polymerization runs with ((Me)$_2$TPL):($^t$Bu–P$_4$) = 6,400:1 in parallel reaction vessels and terminated both reactions simultaneously via precipitation into two different solvents, non-protic hexane and protic methanol, respectively, yielding similar molar mass *l*-P3T(Me)$_2$P ($M_n$ = 2.17 MDa, $Đ$ = 1.26) and *c*-P3T(Me)$_2$P ($M_n$ = 2.23 MDa, $Đ$ = 1.34) (Supplementary Figs. 19 and 20). It is worth mentioning these molar masses were determined absolutely via the use of d$n$/d$c$ values obtained independently for both *l*- and *c*-P3T(Me)$_2$P samples. As is consistent with previous literature[32], the d$n$/d$c$ of *l*-P3T(Me)$_2$P (0.1171 ml g$^{-1}$) was higher than that of its cyclic analogue (0.1107 ml g$^{-1}$) (Supplementary Figs. 21 and 22). These samples were further characterized and compared through analysis of their [$\eta$] and bulk rheological viscosity $\eta$. As expected, *c*-P3T(Me)$_2$P had lower $\eta$ and [$\eta$] (Fig. 3b and Supplementary Fig. 23) as cyclic polymers have a lower degree of chain entanglement[30,32]. Comparing the $M_w$ per elution volume (as functions of hydrodynamic radius), it was found that *c*-P3T(Me)$_2$P on average had $M_w$ a factor of 1.58 times higher than *l*-P3T(Me)$_2$P (Supplementary Fig. 24). Additionally, the radius of gyration ($R_g$) was measured through multiangle light scattering and compared between the linear and cyclic polymers. To measure the mean square radius of gyration ratio more accurately, we first synthesized *l*-P3T(Me)$_2$P ($M_n$ = 2.17 MDa) through quenching in hexanes; it was then redissolved in dichloromethane (DCM) and precipitated in methanol to obtain *c*-P3T(Me)$_2$P ($M_n$ = 2.22 MDa). The *c*/*l* $R_g$ ratio was found to be 0.84 for these UHMM polymers (Fig. 3c) and decreased to 0.71 (Supplementary Fig. 26) for much lower molar mass samples: *c*-P3T(Me)$_2$P, $M_n$ = 18.0 kDa; *l*-P3T(Me)$_2$P, $M_n$ = 18.5 kDa. We reasoned that this observed effect of molar mass on the $R_g$ ratio was because the longer the chains, the lower the differences in rheology and viscosity between cyclic and linear chains, especially in the UHMM region (the model of an infinite linear chain is just that of the cyclic chain). AFM microscopy was selected as the preferred imaging technique, as this method of direct imaging does not require additional modification of polymer chains by way of postpolymerization functionalization or staining typically required for observation[32,34]. Thus, owing to its sulfur-containing and UHMM, direct visualization of the cyclic topology became possible by AFM, which was used to directly image the UHMM *c*-P3T(Me)$_2$P sample, revealing rings of on average roughly 517 nm in diameter, and this again directly supports the cyclic topological assignment (Fig. 3d). At the same time, UHMM *l*-P3T(Me)$_2$P showed completely different, linear morphology through characterization by AFM (Fig. 3e). However, the conditions used for sample preparation (1.0 mg ml$^{-1}$ concentration and 2,000 rpm spin coating speed) yielded polymer aggregates as indicated by the height of around 77 nm for *c*-P3T(Me)$_2$P and roughly 34 nm for *l*-P3T(Me)$_2$P. To reduce or suppress polymer aggregation, we reduced the polymer concentration to 0.01 mg ml$^{-1}$ and increased the speed of spin coating to 4,000 rpm. The resulting AFM images of both cyclic and linear polymers showed a much-reduced height to only about 3.5 nm for *c*-P3T(Me)$_2$P and *l*-P3T(Me)$_2$P (Fig. 3f–i), which is consistent with the height scale for single polymer chains[56]. Overall, coupled with the above-described MALDI–TOF–MS, NMR and SEC results, the collective AFM images fully support our topological assignments, both directly through the observation of aggregate and single chains.

The above results fully support the linear and cyclic structures of UHMM P3T(Me)$_2$P initiated by $^t$Bu–P$_4$ and quenched with non-protic hexane or protic MeOH, respectively, and demonstrate that the protic quench is the key step in enabling the linear-to-cyclic topological transformation. The results and above-described reasonings led to a proposed mechanism, shown in Fig. 1c, that the protic quench triggers the ring closing cyclization event and subsequent displacement of the initiating $^t$Bu–P$_4$ end group. The inability of the propagating zwitterionic P$_4^+$–S$^-$ species to cyclize during polymerization can be attributed to the exceptionally steric hindrance of the P$_4^+$ (~1.4 nm) that effectively blocks intramolecular nucleophilic attack by the terminal sulfide anion S$^-$ and poor leaving nature of $^t$Bu–P$_4$. The same reasoning applies to the postpolymerization quench with hexane. By contrast, quenching with MeOH provides a protic source that triggers the cyclization, as $^t$Bu–P$_4$ is a superbase that favours the abstraction of proton from MeOH to $^t$Bu–P$_4$, yielding [P$_4$H]$^+$[OMe]$^-$, causing detachment of the P$_4$ from the chain and concomitant ring closure (Fig. 1c). Considering that an equilibrium for potential proton exchange between the sulfide and methoxide anions should lie far to the MeOH + sulfide since the p$K_a$ of methyl mercaptan (10.4) is much smaller than that of methanol (24.0), there should be mainly sulfide anions in the system on addition of MeOH. Regarding the observed apparently exclusive selectivity for the intramolecular cyclization over the possible competing intermolecular coupling, we posit that it is due to the combination of the ionic interactions between the termini of the zwitterionic polymer chain and favoured entropy for cyclization via intramolecular ion pairing

https://doi.org/10.1038/s41557-024-01511-2

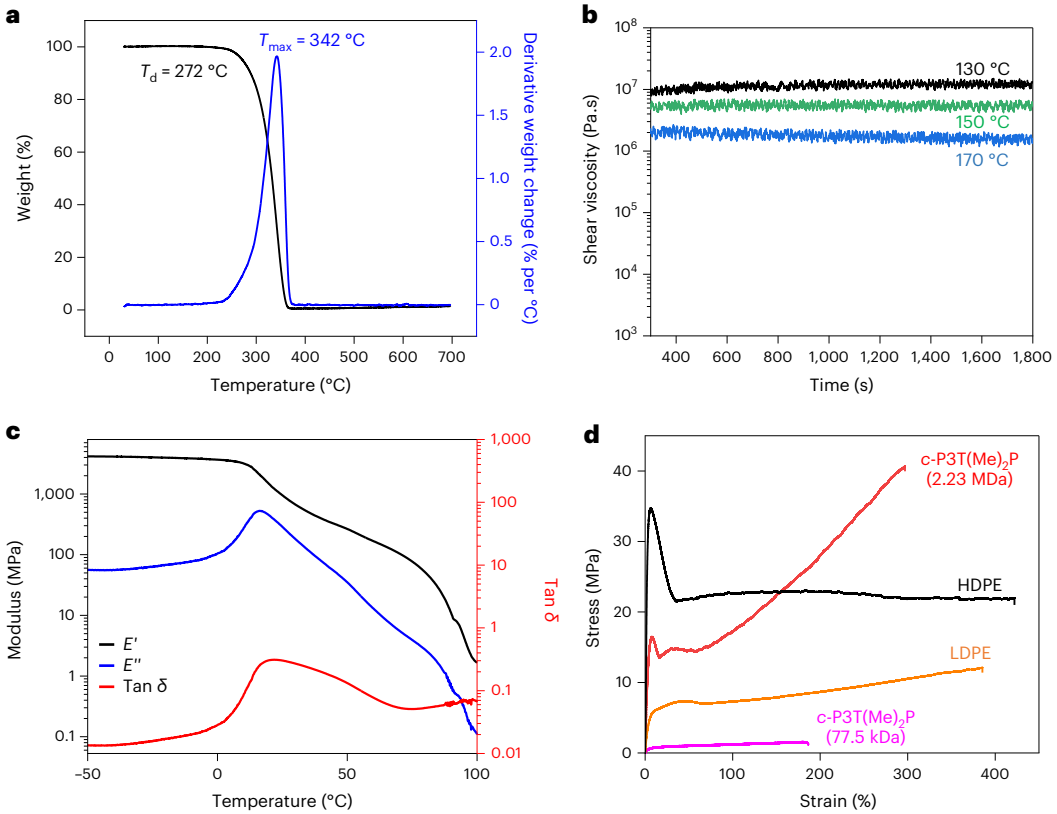


**Fig. 4 | Thermal, rheological and mechanical properties of *c*-P3T(Me)$_2$P.** **a**, TGA and derivative thermogravimetric curves for UHMM *c*-P3T(Me)$_2$P ($M_n$ = 2.23 MDa). **b**, Overlays of shear viscosity in melt (shear rate $\dot{\gamma}$ = 0.01 s$^{-1}$): UHMM *c*-P3T(Me)$_2$P (2.23 MDa, 130 °C, black; 150 °C, green; 170 °C, blue). These plots demonstrate the melt processability of UHMM *c*-P3T(Me)$_2$P. **c**, Overlays of storage modulus *E*′, loss modulus *E*″ and tan δ for UHMM *c*-P3T(Me)$_2$P measured by DMA (tension film mode, 0.05% strain, 1 Hz, 3 °C min$^{-1}$). **d**, Stress–strain curve overlays of UHMM *c*-P3T(Me)$_2$P ($M_n$ = 2.23 MDa) and *c*-P3T(Me)$_2$P ($M_n$ = 77.5 kDa) with LDPE (melt-flow index 7.5) and HDPE (melt-flow index 7.6). The impact of molar mass on mechanical properties is pivotal, with UHMM *c*-P3T(Me)$_2$P demonstrating high ultimate strength and elongation at break.

as the coupling of two polymer chains via intermolecular ion pairing further reduces the total number of microstates (that is, the loss of translational freedom) by a greater amount than cyclization does.

## Thermal, rheological and mechanical properties

Thermal properties of UHMM *c*-P3T(Me)$_2$P ($M_n$ = 2.23 MDa) were first characterized using differential scanning calorimetry (DSC) and thermogravimetric analysis (TGA). Despite having a moderate melting-transition temperature ($T_m$) of 76/83 °C (from the first heating scan, not observable on the second heating scan) and glass-transition temperature ($T_g$) of −1.1 °C (from the second heating scan, unclear on the first heating scan) for *c*-P3T(Me)$_2$P (Supplementary Fig. 28), it exhibited a higher degradation temperature ($T_d$) (the temperature at 5% weight loss) value of 272 °C and maximum rate decomposition temperature ($T_{max}$) of 342 °C (Fig. 4a, Supplementary Fig. 31) compared to that of *c*-P3TB[43] without the dimethyl substituents ($T_d$ = 198 °C). This 74 °C increase in $T_d$ can be attributed to the absence of α-hydrogens that promote *cis*-elimination at high temperatures[49] and leads to a larger processing window (difference between $T_m$ and $T_d$) of 191 °C. Although the topology and molar mass (within the current high molecular region from 129 kDa to 2.23 MDa) were found to have a little effect on $T_m$ (Supplementary Figs. 28–30), the topology showed a greater effect on $T_d$. The $T_d$ of *l*-P3T(Me)$_2$P ($M_n$ = 2.17 MDa) decreased by 14 °C to a lower $T_d$ of 258 °C (Supplementary Fig. 32), attributable to the presence of chain ends. Thermal stability of UHMM *c*-P3T(Me)$_2$P was further evaluated by examining its melt processability through shear viscosity measurements over a period of 30 min at a fixed shear rate and under continuous-flow mode. The shear viscosity remained constant without any obvious decrease at 130 or 150 °C, but at 170 °C there was a slight drop in shear viscosity after 30 min (Fig. 4b), which may indicate the upper limit of the processing temperature.

Thermomechanical properties were examined by dynamic mechanical analysis (DMA), which revealed a high storage modulus (*E*′) value of 3.66 GPa at 0 °C (the glassy state) and a drop in *E*′ after the glass-transition region with an α transition temperature of around 20 °C, as defined by the peak maxima of tan *δ* (the loss modulus (*E*″) to storage modulus ratio (*E*″/*E*′)) (Fig. 4c). Uniaxial tensile testing of dog-bone-shaped specimens of UHMM *c*-P3T(Me)$_2$P ($M_n$ = 2.23 MDa), which were compression moulded via hot pressing at 150 °C, followed by slow cooling and annealing at room temperature for 24 h, revealed a high ultimate strength (*σ*) of 39.3 ± 2.9 MPa, a good elongation at break ($\varepsilon_b$) of 282 ± 14% and an elastic modulus (*E*) of 0.51 ± 0.08 GPa, giving rise to a high toughness of $U_T$ = 66 ± 6 MJ m$^{-3}$ (Supplementary Table 2 and Supplementary Fig. 34). These results were obtained from twice-recycled (reprocessed) specimens prepared by compression moulding, demonstrating excellent reprocessability. When compared with low-density polyethylene (LDPE) and high-density polyethylene (HDPE) standards used for comparison, the UHMM *c*-P3T(Me)$_2$P showed similar ductility but much greater ultimate stress due to its pronounced strain hardening (Fig. 4d). Effects of molar mass on the mechanical performance of *c*-P3T(Me)$_2$P are evident as the polymer with a medium molar mass of $M_n$ = 77.5 kDa (*Đ* = 1.31) is only a soft elastomer with elastic stress *σ* below 1.6 MPa and without a yield point (Fig. 4d). Last, transmittance and reflectance properties of UHMM *c*-P3T(Me)$_2$P were analysed using an ultraviolet-visible near-infrared spectrophotometer. The analysis showed that this polymer is optically

https://doi.org/10.1038/s41557-024-01511-2

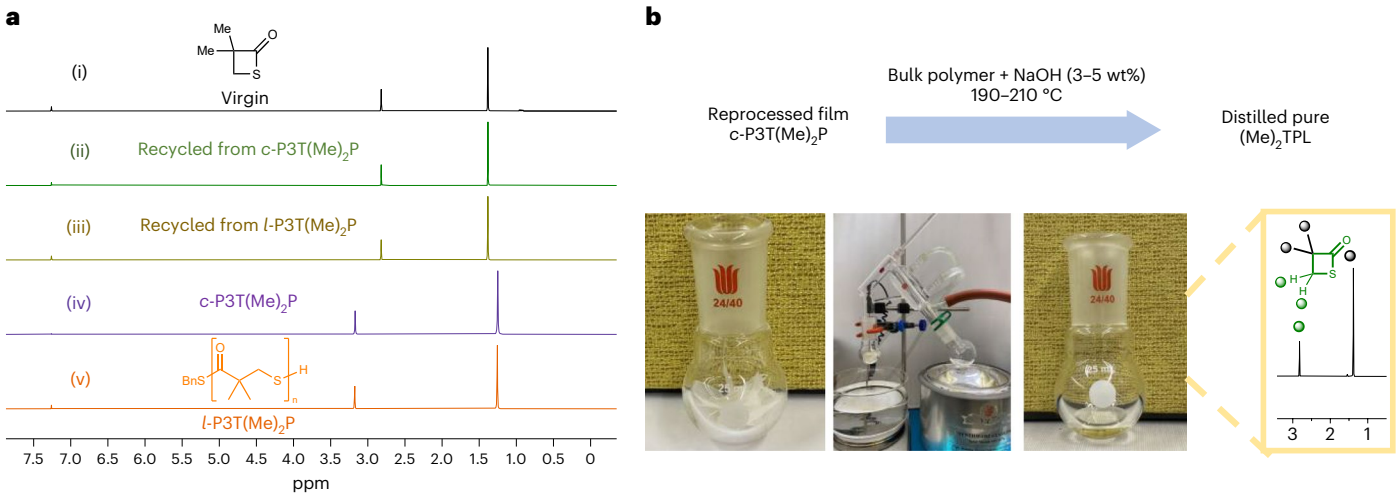


**Fig. 5 | Chemical recycling to monomer. a**, Overlays of $^1$H NMR spectra (23 °C, $CDCl_3$, with residual solvent peak at 7.26 ppm for $CHCl_3$), (i) virgin $(Me)_2$TPL, (ii) the recovered monomer after depolymerization of *c*-P3T$(Me)_2$P ($M_n$ = 36.7 kDa, $Đ$ = 1.27), (iii) the recovered monomer after depolymerization of *l*-P3T$(Me)_2$P ($M_n$ = 24.4 kDa, $Đ$ = 1.49), (iv) virgin *c*-P3T$(Me)_2$P and (v) virgin *l*-P3T$(Me)_2$P. **b**, Visual representation of the depolymerization of reprocessed *c*-P3T$(Me)_2$P film that was depolymerized with 3–5 wt% NaOH at 190–210 °C under vacuum to recover $(Me)_2$TPL.

clear, with a transmittance value ($T$%) of 84% and a reflectance value of 9.0% in the visible range (350–800 nm). Compared to other commercially available materials, this UHMM cyclic polymer is as good as a roughly 3.79 l (1 gallon) Ziploc bag (LDPE, $T$% = 89%), and far superior to highly crystalline isotactic poly(3-hydroxybutyrate) ($T$% =19%) (Supplementary Fig. 35). Last, these properties of UHMM *c*-P3T$(Me)_2$P were also compared with those of UHMM *l*-P3T$(Me)_2$P. Before testing, the topological stability of the zwitterionic *l*-P3T$(Me)_2$P under processing conditions (hot press at 150 °C for 15 min) was verified by observing no change in the integration ratio of the relevant $^1$H NMR peaks of the $P_4$ chain end to the polymer main chain before and after processing (Supplementary Fig. 36). The test results showed that UHMM *c*-P3T$(Me)_2$P ($M_n$ = 2.23 MDa, $Đ$ = 1.34) exhibits similar properties to *l*-P3T$(Me)_2$P ($M_n$ = 2.01 MDa, $Đ$ = 1.35) in transmittance, reflectance and elongation at the break (Supplementary Figs. 37–39), but *c*-P3T$(Me)_2$P displays higher storage and loss moduli in the glassy state by DMA and higher yield stress and ultimate strength by tensile testing (Supplementary Table 3 and Supplementary Figs. 39 and 40).

### Chemical circularity of *c*-P3T$(Me)_2$P

The prospect of chemical recycling to monomer towards establishing a closed-loop lifecycle for *c*-P3T$(Me)_2$P was investigated by chemically catalysed thermolysis or chemolysis (Supplementary Table 4). Heating *c*-P3T$(Me)_2$P ($M_n$ = 36.7 kDa, $Đ$ = 1.27), obtained with $((Me)_2TPL)$:($^t$Bu–$P_4$) = 200:1, mixed with 5 wt% NaOH at 190 °C for 6 h under solvent-free, vacuum (~0.2 Torr) conditions distilled off pure thiolactone monomer $(Me)_2$TPL in a 90% isolated yield (Fig. 5a(ii)). Likewise, a *l*-P3T$(Me)_2$P sample ($M_n$ = 24.4 kDa, $Đ$ = 1.49) was also effectively depolymerized under the same conditions to recover pure $(Me)_2$TPL in a 91% isolated yield (Fig. 5a(iii)). Furthermore, the ceiling temperature ($T_c$) of *c*-P3T$(Me)_2$P was determined by measuring equilibrium monomer concentration $((Me)_2TPL)_{eq}$ at different temperatures through a variable-temperature NMR study using a ratio of $((Me)_2TPL)$:($^t$Bu–$P_4$) = 100:1 at $((Me)_2TPL)_0$ = 0.1 mol l$^{-1}$ in toluene-$d_8$. The Van 't Hoff plot of $\ln((Me)_2TPL)_{eq}$ versus $1/T$ from this experiment gave a straight line, from which standard-state thermodynamic parameters were calculated (Supplementary Fig. 41): the enthalpy change ($\Delta H^o_p$) = −34.4 kJ mol$^{-1}$ and the entropy change of polymerization ($\Delta S^o_p$) = −60.9 J mol$^{-1}$ K$^{-1}$. On the basis of the equation $T_c = \Delta H^o_p/(\Delta S^o_p + R\ln((Me)_2TPL)_0)$, $T_c$ was calculated to be 298 °C when extrapolated to $((Me)_2TPL)_0$ = 1.0 mol l$^{-1}$. Owing to the dynamic nature of thioester bonds promoting the equilibrium to shift towards the monomer state under catalysis and vacuum, catalysed depolymerization can be carried out at a much lower temperature of 190 °C, with continuous removal of the reformed monomer using a vacuum distillation setup (Fig. 5b).

The above depolymerization results used a precipitated powder sample before processing. To simulate a sample that has completed a real-world application use cycle, dog-bone-shaped specimens that had undergone mechanical testing were directly depolymerized in the presence of a catalyst (3 wt% solid NaOH). Thus, when using the reprocessed *c*-P3T$(Me)_2$P film material ($M_n$ = 77.5 kDa, $Đ$ = 1.31), $(Me)_2$TPL was distilled off under vacuum at 190 °C, obtaining the pure monomer in 88% isolated yield (Fig. 5b). Notably, when performing depolymerization on a UHMM cyclic P3T$(Me)_2$P film (1.40 g, $M_n$ = 2.23 MDa, $Đ$ = 1.34) with 3 wt% NaOH at 210 °C under vacuum, pure $(Me)_2$TPL was collected in a total yield of 95% (Supplementary Fig. 42). Worth noting also is that, when the recovered $(Me)_2$TPL was subjected to repolymerization through the $^t$Bu–$P_4$-mediated ROP ($((Me)_2TPL)$:($^t$Bu–$P_4$) = 6,400:1) at 70 °C, UHMM cyclic *c*-P3T$(Me)_2$P was again obtained, achieving a similar $M_n$ (2.09 MDa, $Đ$ = 1.39) to that of the virgin polymer synthesized from the staring $(Me)_2$TPL monomer (Supplementary Fig. 43). Comparative thermal (uncatalysed) depolymerizations of *l*-P3T$(Me)_2$P ($M_n$ = 2.17 MDa, $Đ$ = 1.26) and *c*-P3T$(Me)_2$P ($M_n$ = 2.23 MDa, $Đ$ = 1.34) at 210 °C, ~0.2 Torr and fixed time (12 h) revealed that the monomer recovery yield from the linear polymer (85%) is more than twice that from the cyclic counterpart (40%, Supplementary Fig. 44). This result is expected as the linear polymer has chain ends that allow for depolymerization via chain 'unzipping' initiated by the chain-end nucleophiles, whereas the depolymerization of cyclic polymer relies on spontaneous chain scission. Overall, the above results demonstrated the expedient chemical circularity of *c*-P3T$(Me)_2$P and the distinctive topology-dependent depolymerization phenomenon, primarily dictated by the concentration of polymer chain-end nucleophiles that facilitate depolymerization through the proposed chain 'unzipping' process.

## Conclusion

In summary, we introduced a simple, selective method for the synthesis of UHMM (>2 MDa) linear or cyclic polymers, simply by quenching the polymerization reaction with non-protic hexane or protic methanol, while all other reaction conditions and reagents are identical. In essence, we developed a synthetic methodology that allows for the

synthesis of cyclic polymers with the same degree of control, ease and designability as the synthesis of linear polymers.

In the representative ROP of thiolactone $(Me)_2$TPL described herein in detail, the ROP initiated by superbase $^tBu-P_4$ yields either UHMM *l*-P3T$(Me)_2$P ($M_n$ = 2.17 MDa, $Đ$ = 1.26) when quenched in hexane or UHMM *c*-P3T$(Me)_2$P ($M_n$ = 2.23 MDa, $Đ$ = 1.34) when quenched in methanol. Uniquely, in-polymerization macromolecular cyclization, which is challenging to suppress or eliminate in conventional methods for cyclic polymer synthesis, does not occur during the polymerization or postpolymerization quench with non-protic hexane, but, desirably, it occurs instantaneously when quenching the reaction with protic methanol. This unique cyclization mechanism by a protic trigger on demand enabled selective and controlled synthesis of cyclic polymers, just like the way the linear analogues are synthesized, but just with a different quenching reagent or solvent. In addition, the combination of UHMM and sulfur content in *c*-P3T$(Me)_2$P allowed for direct visualization by AFM without the need for postpolymerization functionalization, whereas UHMM endows much enhanced thermostability and mechanical toughness. Furthermore, owing to its *gem*-disubstitution, this UHMM cyclic (or linear) polymer can be quantitatively recycled back to monomer under mild conditions, establishing a circular lifecycle for cyclic polythioester. Our preliminary results also indicate that this simple method can be applied to other polymer types and that comprehensive study is underway and will be reported in due course in future contributions.

## Online content

Any methods, additional references, Nature Portfolio reporting summaries, source data, extended data, supplementary information, acknowledgements, peer review information; details of author contributions and competing interests; and statements of data and code availability are available at https://doi.org/10.1038/s41557-024-01511-2.

## References


1. Tezuka, Y. *Topological Polymer Chemistry: Progress of Cyclic Polymers in Syntheses, Properties, and Functions* (Word Scientific, 2012).
2. Miao, Z. et al. Cyclic polyacetylene. *Nat. Chem.* **13**, 792–799 (2021).
3. Bielawski, C. W., Benitez, D. & Grubbs, R. H. An 'endless' route to cyclic polymers. *Science* **297**, 2041–2044 (2002).
4. Haque, F. M. & Grayson, S. M. The synthesis, properties and potential applications of cyclic polymers. *Nat. Chem.* **12**, 433–444 (2020).
5. Laurent, B. A. & Grayson, S. M. An efficient route to well-defined macrocyclic polymers via 'click' cyclization. *J. Am. Chem. Soc.* **128**, 4238–4239 (2006).
6. Sun, P., Chen, J., Liu, J. A., & Zhang, K. Self-accelerating click reaction for cyclic polymer. *Macromolecules* **50**, 1463–1472 (2017).
7. Kapnistos, M. et al. Unexpected power-law stress relaxation of entangled ring polymers. *Nat. Mater.* **7**, 997–1002 (2008).
8. Pasquino, R. et al. Viscosity of ring polymer melts. *ACS Macro Lett.* **2**, 874–878 (2013).
9. Doi, Y. et al. Melt rheology of ring polystyrenes with ultrahigh purity. *Macromolecules* **48**, 3140–3147 (2015).
10. Gambino, T., Martínez de Ilarduya, A., Alegría, A. & Barroso-Bujans, F. Dielectric relaxations in poly(glycidyl phenyl ether): effects of microstructure and cyclic topology. *Macromolecules* **49**, 1060–1069 (2016).
11. Ziebarth, J. D. et al. Comparison of critical adsorption points of ring polymers with linear polymers. *Macromolecules* **49**, 8780–8788 (2016).
12. Kammiyada, H., Ouchi, M. & Sawamoto, M. A study on physical properties of cyclic poly(vinyl ether)s synthesized via ring-expansion cationic polymerization. *Macromolecules* **50**, 841–848 (2017).
13. Chen, B., Jerger, K., Frechet, J. M. & Szoka, F. C. Jr. The influence of polymer topology on pharmacokinetics: differences between cyclic and linear PEGylated poly(acrylic acid) comb polymers. *J. Control. Release* **140**, 203–209 (2009).
14. Nasongkla, N. et al. Dependence of pharmacokinetics and biodistribution on polymer architecture: effect of cyclic versus linear polymers. *J. Am. Chem. Soc.* **131**, 3842–3843 (2009).
15. Yamamoto, T. & Tezuka, Y. Cyclic polymers revealing topology effects upon self-assemblies, dynamics and responses. *Soft Matter* **11**, 7458–7468 (2015).
16. Arno, M. C. et al. Exploiting topology-directed nanoparticle disassembly for triggered drug delivery. *Biomaterials* **180**, 184–192 (2018).
17. Natansohn, A. & Rochon, P. Photoinduced motions in azo-containing polymers. *Chem. Rev.* **102**, 4139–4175 (2002).
18. Xu, X. et al. The first example of main-chain cyclic azobenzene polymers. *Macromol. Rapid Commun.* **31**, 1791–1797 (2010).
19. Hoskins, J. N. & Grayson, S. M. Synthesis and degradation behavior of cyclic poly(ε-caprolactone). *Macromolecules* **42**, 6406–6413 (2009).
20. Williams, R. J., Dove, A. P. & O'Reilly, R. K. Self-assembly of cyclic polymers. *Polym. Chem.* **6**, 2998–3008 (2015).
21. Josse, T., De Winter, J., Gerbaux, P. & Coulembier, O. Cyclic polymers by ring-closure strategies. *Angew. Chem. Int. Ed.* **55**, 13944–13958 (2016).
22. Chang, Y. A. & Waymouth, R. M. Recent progress on the synthesis of cyclic polymers via ring-expansion strategies. *J. Polym. Sci., Part A: Polym. Chem.* **55**, 2892–2902 (2017).
23. Wang, T.-W. & Golder, M. R. Advancing macromolecular hoop construction: recent developments in synthetic cyclic polymer chemistry. *Polym. Chem.* **12**, 958–969 (2021).
24. Yoon, K. Y. et al. Scalable and continuous access to pure cyclic polymers enabled by 'quarantined' heterogeneous catalysts. *Nat. Chem.* **14**, 1242–1248 (2022).
25. Boydston, A. J., Xia, Y., Kornfield, J. A., Gorodetskaya, I. A. & Grubbs, R. H. Cyclic ruthenium-alkylidene catalysts for ring-expansion metathesis polymerization. *J. Am. Chem. Soc.* **130**, 12775–12782 (2008).
26. Sarkar, S. et al. An $OCO^{3-}$ trianionic pincer tungsten(VI) alkylidyne: rational design of a highly active alkyne polymerization catalyst. *J. Am. Chem. Soc.* **134**, 4509–4512 (2012).
27. Gonsales, S. A. et al. Highly tactic cyclic polynorbornene: stereoselective ring expansion metathesis polymerization of norbornene catalyzed by a new tethered tungsten-alkylidene catalyst. *J. Am. Chem. Soc.* **138**, 4996–4999 (2016).
28. Roland, C. D., Li, H., Abboud, K. A., Wagener, K. B. & Veige, A. S. Cyclic polymers from alkynes. *Nat. Chem.* **8**, 791–796 (2016).
29. Wang, T. W., Huang, P. R., Chow, J. L., Kaminsky, W. & Golder, M. R. A cyclic ruthenium benzylidene initiator platform enhances reactivity for ring-expansion metathesis polymerization. *J. Am. Chem. Soc.* **143**, 7314–7319 (2021).
30. McGraw, M. L., Clarke, R. W. & Chen, E. Y.-X. Synchronous control of chain length/sequence/topology for precision synthesis of cyclic block copolymers from monomer mixtures. *J. Am. Chem. Soc.* **143**, 3318–3322 (2021).
31. McGraw, M. L. et al. Mechanism of spatial and temporal control in precision cyclic vinyl polymer synthesis by Lewis pair polymerization. *Angew. Chem. Int. Ed.* **61**, e202116303 (2022).
32. Song, Y., He, J., Zhang, Y., Gilsdorf, R. A. & Chen, E. Y.-X. Recyclable cyclic bio-based acrylic polymer via pairwise monomer enchainment by a trifunctional Lewis pair. *Nat. Chem.* **15**, 366–376 (2023).

33. Culkin, D. A. et al. Zwitterionic polymerization of lactide to cyclic poly(lactide) by using *N*-heterocyclic carbene organocatalysts. *Angew. Chem. Int. Ed.* **46**, 2627–2630 (2007).
34. Guo, L., Lahasky, S. H., Ghale, K. & Zhang, D. *N*-heterocyclic carbene-mediated zwitterionic polymerization of *N*-substituted *N*-carboxyanhydrides toward poly(alpha-peptoid)s: kinetic, mechanism, and architectural control. *J. Am. Chem. Soc.* **134**, 9163–9171 (2012).
35. Brown, H. A. & Waymouth, R. M. Zwitterionic ring-opening polymerization for the synthesis of high molecular weight cyclic polymers. *Acc. Chem. Res.* **46**, 2585–2596 (2013).
36. Piedra-Arroni, E., Ladaviere, C., Amgoune, A. & Bourissou, D. Ring-opening polymerization with $Zn(C_6F_5)_2$-based Lewis pairs: original and efficient approach to cyclic polyesters. *J. Am. Chem. Soc.* **135**, 13306–13309 (2013).
37. Reisberg, S. H., Hurley, H. J., Mathers, R. T., Tanski, J. M. & Getzler, Y. D. Y. L. Lactide cyclopolymerization kinetics, X-ray structure, and solution dynamics of ($^t$Bu-SalAmEE)Al and a cautionary tale of polymetalate formation. *Macromolecules* **46**, 3273–3279 (2013).
38. Asenjo-Sanz, I., Veloso, A., Miranda, J. I., Pomposo, J. A. & Barroso-Bujans, F. Zwitterionic polymerization of glycidyl monomers to cyclic polyethers with $B(C_6F_5)_3$. *Polym. Chem.* **5**, 6905–6908 (2014).
39. Hong, M. & Chen, E. Y.-X. Completely recyclable biopolymers with linear and cyclic topologies via ring-opening polymerization of gamma-butyrolactone. *Nat. Chem.* **8**, 42–49 (2016).
40. Zhu, J. B., Watson, E. M., Tang, J. & Chen, E. Y.-X. A synthetic polymer system with repeatable chemical recyclability. *Science* **360**, 398–403 (2018).
41. Naruse, K., Takasu, A. & Higuchi, M. Direct observation of a cyclic vinyl polymer prepared by anionic polymerization using N-heterocyclic carbene and subsequent ring-closure without highly diluted conditions. *Macromol. Chem. Phys.* **221**, 2000004 (2020).
42. Li, H., Ollivier, J., Guilaume, S. M. & Carpentier, J.-F. Tacticity control of cyclic poly(3-thiobutyrate) prepared by ring-opening polymerization of racemic β-thiobutyrolactone. *Angew. Chem. Int. Ed.* **58**, 618–623 (2022).
43. Hong, M. & Chen, E. Y.-X. Chemically recyclable polymers: a circular economy approach to sustainability. *Green Chem.* **19**, 3692–3706 (2017).
44. Coates, G. W. & Getzler, Y. D. Y. L. Chemical recycling to monomer for an ideal, circular polymer economy. *Nat. Rev. Mater.* **5**, 501–516 (2020).
45. Jehanno, C. et al. Critical advances and future opportunities in upcycling commodity polymers. *Nature* **603**, 803–814 (2022).
46. Abel, B. A., Snyder, R. L. & Coates, G. W. Chemically recyclable thermoplastics from reversible-deactivation polymerization of cyclic acetals. *Science* **373**, 783–789 (2021).
47. Haussler, M., Eck, M., Rothauer, D. & Mecking, S. Closed-loop recycling of polyethylene-like materials. *Nature* **590**, 423–427 (2021).
48. Jung, M. E. & Piizzi, G. *gem*-Disubstituent effect: theoretical basis and synthetic applications. *Chem. Rev.* **105**, 1735–1766 (2005).
49. Zhou, L. et al. Chemically circular, mechanically tough and melt-processable polyhydroxyalkanoates. *Science* **380**, 64–69 (2023).
50. Xiong, W. et al. Geminal dimethyl substitution enables controlled polymerization of penicillamine-derived β-thiolactones and reversed depolymerization. *Chem.* **6**, 1831–1843 (2020).
51. Stellmach, K. A. et al. Modulating polymerization thermodynamics of thiolactones through substituent and heteroatom incorporation. *ACS Macro Lett.* **11**, 895–901 (2022).
52. Li, X. L., Clarke, R. W., Jiang, J. Y., Xu, T. Q. & Chen, E. Y.-X. A circular polyester platform based on simple gem-disubstituted valerolactones. *Nat. Chem.* **15**, 278–285 (2023).
53. Vazdar, K. et al. Design of novel uncharged organic superbases: merging basicity and functionality. *Acc. Chem. Res.* **54**, 3108–3123 (2021).
54. Schmitt, M., Faliveve, L., Caporaso, L., Cavallo, L. & Chen, E. Y.-X. High-speed organocatalytic polymerization of a renewable methylene butyrolactone by a phosphazene superbase. *Polym. Chem.* **5**, 3261–3270 (2014).
55. Sweeny, W. & Casey, D. J. Propiothiolactone polymers. US patent 3,367,921A (1965).
56. Kumaki, J., Nishikawa, Y. & Hashimoto, T. Visualization of single-chain conformations of a synthetic polymer with atomic force microscopy. *J. Am. Chem. Soc.* **118**, 3321–3322 (1996).

## Methods

### General consideration

All syntheses and manipulations of air- and moisture-sensitive materials were carried out in flamed Schlenk-type glassware on a dual-manifold Schlenk line or in an inert gas ($N_2$)-filled glovebox. High-performance liquid chromatography (HPLC)-grade organic solvents were first sparged extensively with nitrogen during filling 20 l solvent reservoirs and then dried by passage through activated alumina (for THF and DCM) followed by passage through Q-5 supported copper catalyst (for toluene and hexanes) stainless-steel columns. For the THF used in polymerization reactions, HPLC-grade THF was degassed and dried over sodium and benzophenone for 12 h, followed by vacuum distillation.

### Materials

$^t$Bu–$P_4$ (0.8 M in hexane) was purchased from Sigma-Aldrich Chemical Co. and used in a glovebox as received. Benzyl alcohol (BnOH) and 1,8-diazabicyclo[5.4.0]undec-7-ene (DBU) were purchased from Fisher Scientific Co. and Sigma-Aldrich Chemical Co., respectively, purified by distillation over $CaH_2$ and stored over activated Davison 4 Å molecular sieves. Benzyl mercaptan (BnSH) was purchased from TCI Chemical Co. and used in the glovebox as received. Sodium hydrosulfide hydrate, triethylamine and isobutyl chloroformate were purchased from Oakwood Chemical Co., sodium hydroxide was purchased from Fisher Scientific Co. and all were used in the glovebox as received. 3-Chloropivalic acid was purchased from TCI Chemical Co. LDPE (3–4 mm granules, melt-flow index 7.5) and HDPE (2–4 mm granules, melt-flow index 7.6) were purchased from Sigma-Aldrich and Goodfellow, respectively. A roughly 3.79 l (1 gallon) Ziploc bag was purchased from Walmart and tested as purchased. Bacterial *it*-P3HB ($M_n$ = 550 kDa, 5 mm granules, product code BU39-GL-000111) was purchased from Goodfellow.

### Instruments and characterizations

**NMR analysis.** NMR spectra were recorded on a Varian Inova or Bruker AV-III 400 MHz spectrometer (400 MHz, $^1$H; 100 MHz, $^{13}$C) at 298 K. Chemical shifts ($\delta$) are reported in ppm with the solvent resonance used as the internal standard (chloroform-$d_1$ at 7.26 ppm for $^1$H NMR and 77.0 ppm for $^{13}$C NMR; THF-$d_8$ at 3.58 ppm for $^1$H NMR; DCM-$d_2$ at 5.30 ppm for $^1$H NMR). Signals are reported as integration, multiplicity (s, singlet; d, doublet; t, triplet), coupling constant(s) in Hz and assignment.

**Absolute molar mass measurements by SEC.** Measurements of polymer absolute $M_w$, $M_n$ and $Đ$ values were performed by SEC on an Agilent HPLC system equipped with one guard column and two PLgel 5 µm mixed-C gel permeation columns, and coupled with a Wyatt DAWN HELEOS II multi (18)-angle light scattering detector and a Wyatt Optilab TrEX dRI detector. The analysis was performed at 40 °C using $CHCl_3$ as the eluent at a flow rate of 1.0 ml min$^{-1}$, using Wyatt ASTRA v.7.1.2 molar mass characterization software. Viscometry experiments were performed in a similar way with the addition of a Wyatt Viscostar III viscometer. Polymer solutions were prepared in $CHCl_3$ and injected into a dRI detector by the Harvard Apparatus pump 11 at a flow rate of 0.2 ml min$^{-1}$. A series of known concentrations were injected and the change in refractive index was measured to obtain a plot of change in refractive index versus change in concentration ranging from 0.5 to 10.0 mg ml$^{-1}$. The slope from a linear fitting of the data was the d$n$/d$c$ of the polymer: d$n$/d$c$ = 0.1171 ± 0.0029 ml g$^{-1}$ for *l*-P3T(Me)$_2$P and d$n$/d$c$ = 0.1107 ± 0.0019 ml g$^{-1}$ for *c*-P3T(Me)$_2$P.

**MALDI–TOF–MS.** The experiment was performed on a Bruker Ultraflextreme mass spectrometer (Bruker Daltonics) operated in positive ion, reflector mode using a Nd:YAG laser at 355 nm and 20 kV accelerating voltage. A thin layer of a mixed solution (20 µl of 20 g l$^{-1}$ *trans*-2-(3-(4-*tert*-butyphenyl)-2-methyl-2-propenylidene)malononitrile in THF, 3 µl of 10 g l$^{-1}$ polymer sample, 1 µl of 22.1 g l$^{-1}$ sodium trifluoroacetate) was deposited on the target plate (ground steel). Polyethylene glycol (4 kDa) was used as the calibrant and prepared the same way as the polymer sample. The raw data were processed using FlexAnalysis (v.3.4.7, Bruker Daltonics).

**DSC and TGA.** Melting-transition ($T_m$) and glass-transition ($T_g$) temperatures were measured by DSC on an Auto Q20, TA Instruments. All $T_m$ and $T_g$ values were obtained from the second scan unless indicated otherwise. Both heating rate and cooling rate were 10 °C min$^{-1}$ unless indicated otherwise. Decomposition temperatures ($T_d$) and maximum rate decomposition temperatures ($T_{max}$) of the polymers were measured by TGA on a Q50 TGA Analyzer, TA Instruments. Polymer samples were heated from ambient temperature to 700 °C at a heating rate of 10 °C min$^{-1}$. Values of $T_{max}$ were obtained from derivative thermogravimetric curve: wt%/°C versus temperature (°C) plots.

**Mechanical analysis.** Tensile stress–strain testing was performed by an Instron 5966 universal testing system (10 kN load cell) on dog-bone-shaped test specimens (ASTM D638 standard; Type V) prepared via compression moulding using a Carver Bench Top Laboratory Press (model no. 4386) equipped with a two-column hydraulic unit (Carver, model 3912, maximum force 24,000 psi) unless indicated otherwise. Isolated polymer materials were loaded between non-stick Teflon paper sheets into a stainless-steel mould with inset dimensions 30 × 73.5 × 0.38 mm$^3$ fabricated in-house and compressed between two 1.8 × 1.8 m$^2$ (6 × 6 feet$^2$) steel electrically heated platens at a clamp force of 5,000 psi and at a temperature 10 °C higher than each material's respective $T_m$. Specimens for analysis were generated via compression moulding and cut using an ASTM D638-5-IMP cutting die (Qualitest) to standard dimensions. Mechanical behaviour was averaged for all the specimens measured for each individual species investigated. Thickness (0.38 ± 0.01 mm), width (3.18 mm) and grip length (26.4 ± 0.2 mm) of the measured dog-bone specimens were measured for normalization of data by the Bluehill measurement software (Instron). Test specimens were affixed into the screw-tight grip frame. Tensile stress and strain were measured to the point of material break at a grip extension speed of 5.0 mm min$^{-1}$ at ambient conditions. Testing of control standards of commercial HDPE and LDPE for comparative stress–strain curves included in Fig. 4d. The detailed tensile testing results (individual stress–strain curves and tables) were previously reported in ref. 52 and the values were taken from that paper for comparison while plotting overlay Fig. 4d in the main text.

**Rheology experiments.** Shear viscosity measurements were performed on a Discovery Series HR-2 hybrid rheometer (TA Instruments) under nitrogen gas flow (30 psi). Test specimens were loaded between two 8 mm steel electrically heated platen loading discs. Test specimens were trimmed at predetermined temperatures above the $T_m$ of respective polymers. The measurements were performed at gap lengths around 600 µm and an experimental axial force of roughly 0.2 N. The shear viscosity (in melt) over time experiment was performed under flow mode with a shear rate $\dot{\gamma}$ = 0.01 s$^{-1}$ and a duration time of 1,800 s.

**Rheology–viscosity experiments.** Viscosity experiments by rheology were performed on thoroughly dried linear and cyclic polymers prepared by heated compression moulding at 150 °C (between two steel plates, a 38.1 × 12.7 × 1 mm$^3$ steel mould, and non-stick Teflon sheets) inside a Carver Bench Top Laboratory Press (model 4386). Small circular-cut (8 mm diameter) samples were loaded between two 8 mm steel S6 electrically heated platen loading discs within a Discovery Series HR-2 (Hybrid Rheometer) (TA Instruments) under nitrogen gas flow (30 psi) connected to the TRIOS software (TA Instruments). Viscosity was studied under the flow testing option and amplitude setting. Experiments were run at 150 °C with shear rates varying between $10^{-3}$

and 10 rad $s^{-1}$. The axial force was controlled within a negligible ±0.1 N to prevent non-frictional forces.

**AFM.** AFM images were obtained under ambient conditions using a Bruker Bioscope Resolve AFM in Peak Force Tapping Scanasyst mode. Silicon cantilevers (SCANASYST-AIR, spring force constant 0.12 N $m^{-1}$, frequency 23 kHz) were used. The samples were prepared under ambient conditions by spin coating (2,000 or 4,000 rpm, 30 s) freshly cleaved sheets (5 $mm^2$) of highly ordered pyrolytic graphite with 10 µl of thoroughly dissolved polymer samples (1 or 0.01 mg $ml^{-1}$ in toluene).

**DMA.** Storage modulus ($E'$), loss modulus ($E''$) and tan $\delta$ ($E''/E'$) were measured on a Q800 DMA Analyzer (TA Instruments) in a tension film mode at a maximum strain of 0.05% and a frequency of 1 Hz (complying with strain-sweep and frequency-sweep linearity analysis performed before sample testing). Specimens for analysis were generated via compression moulding and cut down to a standard width (13 mm). Specimen length (5–10 mm) and thickness (0.85 ± 0.01 mm) were measured for normalization of data by Q-series measurement software (TA Instruments). Test specimens were mounted to screw-tight grips (maximum 2 N). The samples were heated from −50 to 100 °C at a heating rate of 3 °C $min^{-1}$. The α-transition temperature was calculated as the peak maxima of the tan $\delta$ curve. Samples were tested to the point of yield (amplitude of displacement >20 mm) with measurements repeated for three specimens, the values reported are averaged from the measured data.

**Ultraviolet-visible light-near-infrared optical property measurements.** A Cary 5000 ultraviolet-visible light-near-infrared spectrophotometer from Agilent was used to measure the optical properties of thin films that were acquired by solvent casting from a suitable solvent. The films were cast in circular Teflon petri dish with a diameter of 6.5 cm. Film thickness was measured to be 0.02 ± 0.01 mm. Films were acquired by solvent casting from an appropriate solvent that was allowed to evaporate overnight and covered by tin foil with small holes to allow for slow evaporation before testing.

**Procedures for the synthesis of *l*- and *c*-P3T(Me)$_2$P.** The ROP reactions were performed in 10 ml Schlenk flasks or in 5.5 ml glass reactors inside an inert glovebox at ambient temperature (~23 °C). A predetermined amount of $(Me)_2$TPL was added to a base catalyst solution in THF, or to a mixture of base catalyst and alcohol initiator in THF (as indicated in the polymerization tables) that was stirred at ambient temperature for 10 min before addition of monomer. The sealed reactors were taken out of the glovebox and stirred at 70 °C. After a desired period, a graduate change in viscosity was observed, and an aliquot was taken from the reaction mixture and prepared for $^1$H NMR analysis to obtain the percentage monomer conversion data. For reactions with (DBU):(BnSH) to obtain linear polymer, the polymerization was quenched by addition of benzoic acid in chloroform (5 mg $ml^{-1}$), followed by precipitation in excess methanol 2–3 times. For the reactions with $^t$Bu–$P_4$ to obtain *l*-P3T$(Me)_2$P, the polymerization was precipitated in excess hexane 2–3 times. For reactions with $^t$Bu–$P_4$ to obtain *c*-P3T$(Me)_2$P, the polymerization was quenched by addition of benzoic acid in chloroform (5 mg $ml^{-1}$) and precipitated in excess methanol 2–3 times, or directly precipitated into methanol without addition of benzoic acid in chloroform. All precipitated polymers were then isolated by filtration, and the white polymer solid was dried in a vacuum oven at 60 °C to a constant weight.

### Chemical recycling to lactone monomers $(Me)_2$TPL and repolymerization

For freshly precipitated *c*- or *l*-P3T$(Me)_2$P, NaOH (5.0 mg, 5 wt%) and *c*- or *l*-P3T$(Me)_2$P (0.116 g, 1 mmol) obtained with a ($(Me)_2$TPL):($^t$Bu–$P_4$) ratio of 200:1 or ($(Me)_2$TPL):(DBU):(BnSH) ratio of 200:1:1 was added to a 5.5 ml glass reactor with a stir bar. The mixture was heated at 190 °C (oil bath) and the reformed monomer was distilled off under vacuum (~0.2 Torr) with a receiving flask cooled to −78 °C (dry ice and acetone). After the polymer solid disappeared (about 6 h), the vacuum was turned off and the cold bath was removed. As the flask was warmed to room temperature, a liquid was obtained, which was confirmed to be the recycled, pure monomer $(Me)_2$TPL by $^1$H NMR analysis at 90–91% isolated yields.

For a reprocessed film of *c*-P3T$(Me)_2$P ($M_n$ = 77.5 kDa, $Đ$ = 1.31; cut into small pieces with scissors): NaOH (39 mg, 5 wt%) and *c*-P3T$(Me)_2$P (1.30 g, 11.2 mmol) obtained with a ($(Me)_2$TPL):($^t$Bu–$P_4$) ratio of 400:1 was added to a 25 ml flask with a stir bar. The mixture was heated at 190 °C (oil bath) and the reformed monomer was distilled off under vacuum (~0.2 Torr) with a receiving flask cooled to −78 °C (dry ice and acetone). After the polymer solid disappeared (about 6 h), the vacuum was turned off and the cold bath was removed. As the flask was warmed to room temperature, a liquid was obtained, which was confirmed to be the recycled, pure monomer $(Me)_2$TPL by $^1$H NMR analysis at 88% isolated yield.

For a thin film of *c*-P3T$(Me)_2$P ($M_n$ = 2.23 MDa, $Đ$ = 1.34; cut into small pieces with scissors): NaOH (42 mg, 3 wt%) and *c*-P3T$(Me)_2$P (1.40 g, 12.1 mmol) obtained with a ($(Me)_2$TPL):($^t$Bu–$P_4$) ratio of 6,400:1 was added to a 25 ml bottle with a stir bar. The mixture was heated at 210 °C (oil bath) and distilled off under vacuum (~0.2 Torr) with a receiving flask cooled to −78 °C (dry ice and acetone). After the polymer solid disappeared (10 h), the vacuum was turned off and the cold bath was removed. As the flask was warmed to room temperature, a liquid was obtained, which was confirmed to be the recycled, pure monomer $(Me)_2$TPL by $^1$H NMR analysis at 95% isolated yield.

The recovered $(Me)_2$TPL monomer was filtered through a layer of silica gel (pentane:acetone at 50:1), and the filtrate was concentrated, then added $CaH_2$ and distilled. The distilled monomer was repolymerized with the same polymerization procedure as the virgin monomer to obtain UHMM *c*-P3T$(Me)_2$P with a similar $M_n$ (2.09 MDa, $Đ$ = 1.39) to that of UHMM *c*-P3T$(Me)_2$P synthesized from the starting $(Me)_2$TPL monomer.

**Synthesis, tables, spectra and plots.** Detailed procedures of the synthesis of the monomer and the results of polymerization and depolymerization reactions summarized in tables and spectra, as well as additional polymer characterization data, are provided in the respective sections of the Supplementary Information.

## Data availability

Full experimental details and the data supporting the findings of this study are available within the article and its Supplementary Information. Source data are provided with this paper.

## Acknowledgements

Funding was provided by the US Department of Energy, Office of Energy Efficiency and Renewable Energy, Advanced Materials and Manufacturing Technologies Office (AMMTO) and Bioenergy Technologies Office (BETO). This work was performed as part of the Bio-Optimized Technologies to keep Thermoplastics out of Landfills and the Environment (BOTTLE) Consortium and was supported by AMMTO and BETO under Contract DE-AC36-08GO28308 with the National Renewable Energy Laboratory, operated by Alliance for Sustainable Energy, LLC. The BOTTLE Consortium includes members from Colorado State University. The work by L.T.R. and E.Y.-X.C. was supported by the US National Science Foundation (grant no. NSF-2305058). We thank R. R. Gowda for d*n*/dc measurements.

## Author contributions

E.Y.-X.C. conceived the project and directed the research. L.Z., L.T.R., C.S. and E.C.Q. designed and conducted experiments and analysed the results. L.Z. wrote the initial paper, L.T.R. and E.C.Q. contributed to subsequent versions. E.Y.-X.C. edited the initial and subsequent versions and reviewed the entire paper.

## Competing interests

E.Y.-X.C. and L.Z. are named inventors on a pending PCT/US patent application (2023/021512) submitted by Colorado State University, which covers chemically circular polymers. The other authors declare no competing interests.

## Additional information

**Supplementary information** The online version contains supplementary material available at https://doi.org/10.1038/s41557-024-01511-2.

**Correspondence and requests for materials** should be addressed to Eugene Y.-X. Chen.

**Peer review information** *Nature Chemistry* thanks Matthew Golder, Sophie Guillaume, Julia Pribyl Ham and the other, anonymous, reviewer(s) for their contribution to the peer review of this work.